Journal of Magnetic Resonance **146,** 49–57 (2000)
doi:10.1006/jmre.2000.2112, available online at http://www.idealibrary.com on IDEAL®

In Vitro Monitoring of Total Choline Levels in a Bioartificial Pancreas: ^{1}H NMR Spectroscopic Studies of the Effects of Oxygen Level

Robert C. Long, Jr.,* Klearchos K. Papas,†,[1] Athanassios Sambanis,† and Ioannis Constantinidis*

**Frederik Philips Magnetic Resonance Research Center, Department of Radiology, Emory University School of Medicine, Atlanta, Georgia 30322; and †School of Chemical Engineering and P. H. Petit Institute for Bioengineering and Bioscience, Georgia Institute of Technology, Atlanta, Georgia 30332*

Received October 18, 1999; revised April 27, 2000

This investigation implements specifically designed solvent-suppressed adiabatic pulses whose properties make possible the long-term monitoring of ^{1}H NMR detectable metabolites from alginate/poly-L-lysine/alginate (APA)-encapsulated βTC3 cells. Our encapsulated preparations were maintained in a perfusion bioreactor for periods exceeding 30 days. During this prolonged cultivation period, the cells were exposed to repetitive hypoxic episodes of 4 and 24 h. The ratio of the total choline signal (3.20 ppm) to the reference signal (observed at 0.94 ppm assigned to isoleucine, leucine, and valine) decreased by 8–10% for the 4-h and by 20–32% for the 24-h episodes and returned to its prehypoxic level upon reoxygenation. The decrease in the mean value of total choline to reference signal ratio for three 4-h and two 24-h episodes in two different cultures was highly significant ($P < 0.01$). The rate of recovery by this ratio was slower than the rates of recovery by oxygen consumption, lactate production, or glucose consumption. A step-up in oxygen level led to a new, higher value for the total choline to reference ratio. From spectra of extracts at 400 MHz, it was determined that 63.6% of the total choline signal is due to intracellular phosphorylcholine. Therefore, it is inferred that the observed changes in total choline signal are linked to an oxygen level dependence of the intracellular phosphorylcholine. Several possible mechanisms in which oxygen may influence phosphorylcholine metabolism are suggested. In addition, the implications of these findings to the development of a noninvasive monitoring method for tissue-engineered constructs composed of encapsulated cells are discussed. © 2000 Academic Press

Key Words: **^{1}H NMR; βTC3 insulinoma cells; hypoxia; total choline.**

INTRODUCTION

The noninvasive *in vivo* monitoring of biochemical processes relevant to the function, survival, and longevity of tissue-engineered pancreatic constructs is extremely important for the development of the optimum construct design. This study represents the first step toward establishing a noninvasive *in vivo* monitoring method that utilizes existing magnetic resonance technology and permits the evaluation of key intracellular metabolites in a microencapsulation-based bioartificial pancreas. The model construct employed in this study consists of insulin-secreting βTC3 cells encapsulated in an alginate/poly-L-lysine/alginate (APA) matrix. This matrix imposes a barrier that can be manipulated to have a molecular weight cutoff of approximately 70,000 Da at the time of preparation. Consequently, nutrients and metabolites with smaller molecular weights diffuse through the construct, but antibodies with molecular weights above the cutoff and cytotoxic cells are excluded (*1, 2*). Such constructs provide an elegant model implant that can secrete insulin on demand by sensing the glucose concentration in the surrounding fluid. Similar constructs containing mammalian islets have successfully restored normoglycemia in both small and large animals (*3–7*) and have been somewhat successful in one human patient (*8*) for an extended period of time.

Our previous work has explored important biochemical properties in this type of construct using both traditional biochemical and NMR-based ^{31}P and ^{13}C NMR spectroscopy methods (*9–17*). Specifically, the effects of repetitive exposure to either low or high glucose (basal or stimulated insulin secretion) or hypoxia on the bioenergetic status of the encapsulated cells were investigated. In addition, we established that during prolonged perfusion cultures, APA-entrapped βTC3 cells maintained in a packed-bed bioreactor system undergo significant cell growth (*12*). The profiles of metabolic and secretory activity by the encapsulated cells are characterized by three distinct phases (*12, 16*). Phase 1 (P1) is an initial stable period that lasts for 3–5 days, Phase 2 (P2) is a period of rapid growth that lasts until Days 5–7, and Phase 3 (P3) is a period of metabolic and secretory steady state that is sustained for the remainder of the culture.

Unlike ^{13}C and ^{31}P NMR, ^{1}H NMR spectroscopy has seen limited application for the study of cells (*18–20*) in perfusion bioreactors. Three major causes of this limitation are (1) effective water suppression over the bioreactor volume; (2) the stability of the excitation scheme and quality of the water suppression over repetitive data acquisitions during many days of culture; and (3) achieving a homogeneous B_0 field over the

[1] Currently at Novartis Institute for Biomedical Research, Novartis Pharmaceuticals Corporation, Core Technologies/Analytics-BioNMR, Summit, NJ 07901.

1090-7807/00 $35.00

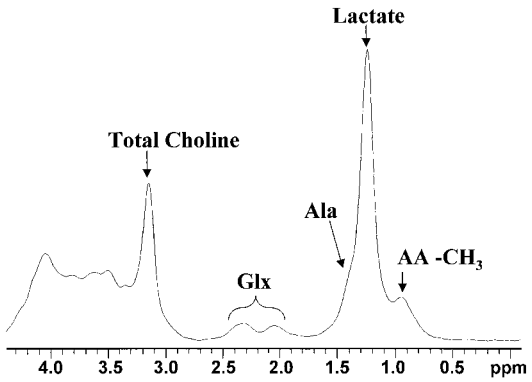

FIG. 1. Water-suppressed proton spectrum (200 MHz) of βTC3 insulinoma cells entrapped in 1.0 ± 0.2 mm APA beads (total volume 22 mL) in a packed-bed bioreactor perfused at 30 mL/min. The repetition time is 2.39 s and the delay between 90° and 180° SSAP pulses, TE/2, is 128 ms. The spectrum represents 64 acquisitions, with a Gaussian line broadening, gf, of 0.038 s defined in $\exp(-(t/\mathrm{gf})^2)$. Total choline = choline + phosphocholine + glycerophosphocholine; Glx = glutamate + glutamine; Ala = alanine; and AA-CH_3 is the reference peak whose intensity is stable throughout the culture period. AA-CH_3 is tentatively assigned to the methyl protons of amino acids leucine, isoleucine, and valine in the growth media.

bioreactor volume. In order to observe intracellular metabolites with millimolar concentrations in the presence of water (concentration of 110 M for hydrogens), it is required that one use optimized pulse sequences to minimize the intensity of the water resonance. Several water-suppression methods are currently being utilized, including presaturation, relaxation-based techniques, and gradient and combined selective-excitation-gradient-based methods. Many of these have been reviewed recently by Gueron *et al.* (*21*).

We have applied specifically designed solvent-suppression adiabatic pulses whose properties make possible the monitoring of ^{1}H NMR detectable metabolites from APA-entrapped βTC3 cells perfused in a packed-bed bioreactor over a prolonged period of time. Periodic application of 1D chemical shift imaging (CSI) has also allowed us to determine changes in the distribution of the detected metabolites along the bioreactor flow axis with the age of culture. In this study, we present data on the relationship between the ^{1}H NMR detectable total choline signal and dissolved oxygen concentration (DO). The implications of our findings to the development of a noninvasive monitoring method for tissue-engineered pancreatic constructs are discussed.

RESULTS

Figure 1 shows a representative ^{1}H NMR spectrum at 200 MHz of APA-encapsulated βTC3 cells perfused with DMEM. Resonance assignments are displayed in the figure and are based on extract spectra and on published values of known chemical shifts (*22*). The resonance at 3.20 ppm is labeled as total choline since it was determined from extract spectra that it is composed of the $-N^+(CH_3)_3$ groups of choline (Cho), phosphorylcholine (PCho), and glycerophosphorylcholine (GPC). For the βTC3 cell line and culture conditions used in this study, extract spectra of monolayer cultures acquired at 400 MHz illustrate that PCho represents the major contributor to this signal with 63.6 ± 4.0% followed by GPC with 33.4 ± 4.0% and Cho with 3.0 ± 0.4%. Upfield of the total choline resonance, the two broad resonances ranging between 2.35 and 2.07 ppm represent a mix of the β- and γ-protons of glutamate and glutamine (Glx), while the large resonance at 1.27 ppm is assigned to the lactate $-CH_3$ group. The shoulder downfield of the lactate peak at 1.43 ppm is assigned to alanine (Ala), while the peak upfield of the lactate resonance at 0.94 ppm is assigned to the methyl resonances of amino acids (labeled AA-CH_3 in Fig. 1). Based on the composition of DMEM and the chemical shifts of the different amino acids, the compounds most likely contributing to this resonance are isoleucine, leucine, and valine. During each experiment described in this study, this resonance remained stable in intensity due to medium replenishment and, as a result, the peak labeled AA-CH_3 in Fig. 1 is used as the "reference" peak in the expression of several ratios presented and discussed below. An external sealed capillary was considered, but the residual air in the capillary caused line broadening of the proton reference signal.

It is possible that additional metabolites may also contribute to the signal intensity of the total choline or lactate resonances. For example, the H-2 protons of β-D-glucose have a chemical shift of 3.24 ppm (it appears as a multiplet) and, therefore, a contribution to the total choline resonance is possible. However, under the present experimental conditions, with the spin echo occurring 128 ms after the refocusing adiabatic pulse, their contribution is minimized due to a combination of T_2 spin relaxation and *J*-modulation effects. Furthermore, spectra acquired from a 50 mM β-glucose solution in the bioreactor in the absence of beads using the same sequence showed negligible intensity from the H-2 resonance (data not shown). Triglycerides from serum in media might be expected to contribute to the signal intensity near the lactate resonance at 1.3 ppm. However, their contribution should be minimized by the long echo time used. This was confirmed by comparison of spectra of cell-free APA beads perfused with either serum-free or serum-supplemented DMEM.

The signals presented in Fig. 1 are a composite of metabolites that are intracellular and extracellular. To determine the compartmentalization of the total choline and lactate peaks, we performed experiments with single-pass perfusion using fresh media. From samples of fresh media, lactate was measured to be 1.2 mM, while choline was assumed to be between 0.025 and 0.032 mM as previously published for serum-supplemented DMEM (*23*). Our NMR data showed that upon switching from recirculation to single-pass perfusion, the lactate signal fell to low levels, whereas the total choline signal remained constant in intensity. Furthermore, the total choline resonance was only observed when data were acquired from

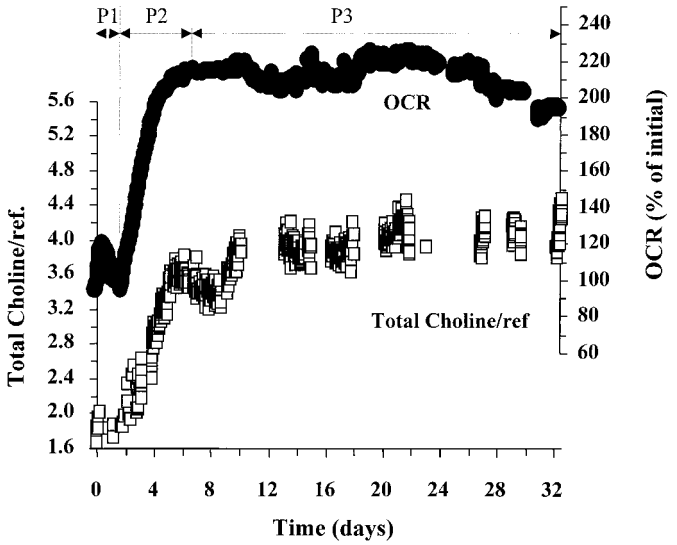

FIG. 2. Temporal profiles of oxygen consumption rate (OCR) (solid circles), depicted as the percentage change from the initial consumption rate, and the ratio of the total choline/reference (total choline/ref) (open squares). The data presented are from Culture I. The three characteristic phases of the culture are P1, P2, and P3. The arrows mark the time duration of each phase.

APA beads that contained cells. Therefore, it was deduced that the origin of the total choline resonance was primarily intracellular, while lactate was primarily extracellular.

Figure 2 shows the temporal changes of the total choline resonance, as well as the rate of oxygen consumption (OCR), by the entire cell population during the lifetime of the 32-day culture. Changes in total choline are presented as the ratio of the fitted area of the total choline peak divided by the area of the "reference" peak, while changes in OCR are presented as percentage change over the initial value of OCR determined during the first few hours of operation. As we have previously demonstrated, cultures of APA-entrapped βTC3 cells undergo three distinct phases in our perfusion system: a lag phase (P1), a growth phase (P2), and a plateau phase (P3) (*12*). Metabolic and secretory indexes, such as the rates of oxygen and glucose consumption, lactate production and insulin secretion, and the intracellular concentration of ATP as measured by ^{31}P NMR spectroscopy for the specific alginate conditions, roughly double between P1 and P3 (*12*). The same pattern of change is also observed in the present cultures. The ratio of total choline to reference indicates that the total choline resonance parallels the metabolic activity of the culture. This change in signal intensity is attributed to a combination of physiologic effects, as well as to a net cell growth. To account for the effects of relaxation times as a potential source of intensity change during the growth history of a culture, experiments reflecting T_1 and T_2 information were performed. Effects of T_1 were ascertained in Culture I by acquiring two data sets, one at a repetition time of 2.39 s and one at 6.39 s on Days 1, 5, 10, 16, and 31. For the total choline, lactate, and the reference signal the ratio of the intensity at 6.39 s to that at 2.39 s was determined for each of these days. The average for the 5 days was 1.18 ± 0.07 for total choline, 1.53 ± 0.08 for lactate, and 1.25 ± 0.07 for the reference peak. Effects of T_2 were measured by acquiring spectra at TE/2 of 128 and 178 ms. The ratio of the intensity at TE/2 of 178 ms to that at 128 ms was evaluated for the total choline, lactate, and reference peaks. Although the signals are not fully relaxed, no statistically significant changes of the above ratios reflecting T_1 or T_2 were observed for the total choline, lactate, or the reference resonance during the time period of the culture.

The effects of DO on the total choline resonance intensity can be attributed to two independent mechanisms: (1) changes in total choline as a result of a change in viable cell number supported by a particular DO level, and (2) changes in total choline as a result of a physiologic or metabolic change for a given viable cell number. Two types of DO experiments were performed to provide information to help deconvolute this potentially complex behavior. In the first experiment, the effect of DO on the total choline intensity for a given viable cell number was determined during transient (4 and 24 h duration) decreases in DO. The duration of these hypoxic episodes was short enough to prevent significant βTC3 cell growth or death during the episode. This was ascertained from the equality of OCR before and after the hypoxic insult in this work and in Ref. (*17*). In total, two 4-h episodes and one 24-h episode were carried out in Culture I. The maximum decrease for the choline/reference ratio during the hypoxic episodes of Culture I were 9.8 and 8.9% for the two 4-h episodes, and 32% for the 24-h episode. When comparing by *t* test the mean of the ratio before and at the end of the hypoxic episodes, these declines were highly significant ($P < 0.001$). Additional 4-h and 24-h episodes were carried out in Culture II. Changes of the choline/reference ratio were barely detectable for the 4-h episode ($P < 0.01$), while for the 24-h episode the ratio was reduced by 19% ($P < 0.001$). The results for the 24-h episode of Culture II are illustrated in Fig. 3. The time variable for these displays starts on Day 6 at the beginning of the P3 period for Culture II. Panel A displays the profile of DO measured at the input ($DO_{(in)}$) and output ($DO_{(out)}$) of the bioreactor as well as the resultant OCR of the culture. OCR, as percentage of initial, starts at ~200% on this display since the cell doubling occurred in P2. It is noteworthy to point out that after each hypoxic exposure, reoxygenation of the culture resulted in an immediate recovery of OCR to its prehypoxic value. This result suggests that the net number of viable cells is unaffected by the hypoxic episode, despite the reduction in metabolic activity during the episode. Panel B displays the profiles for the ratios of total choline to reference and lactate to reference measured by ^{1}H NMR. Induction of hypoxia causes a decrease in the ratio of total choline to reference that continues for the duration of the episode. Upon reoxygenation the ratio begins to recover and reaches its prehypoxic value within ~2 days. Conversely, the lactate ratio increases during hypoxia and recovers to its pre-

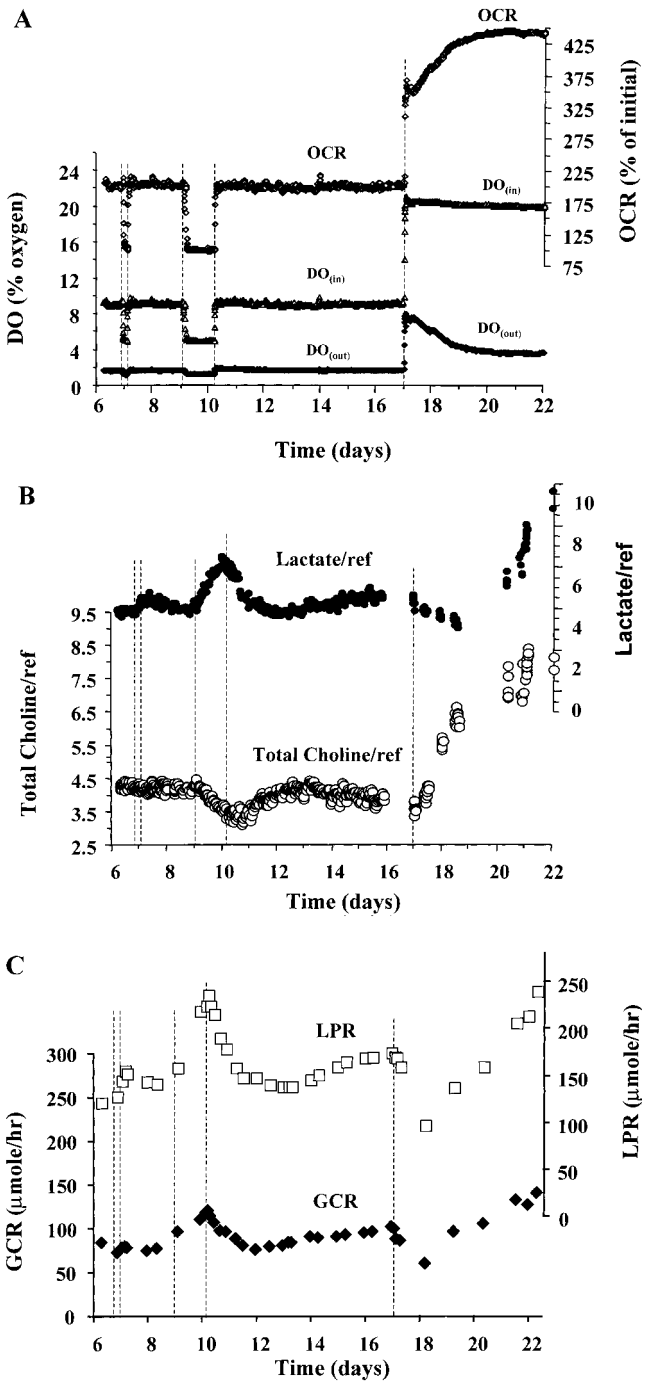

FIG. 3. Temporal profiles of key metabolic and NMR parameters during the steady-state phase, P3, observed from Culture II. (A) Input and output dissolved oxygen levels ($DO_{(in)}$ and $DO_{(out)}$) as percentage oxygen in a gas phase in equilibrium with the liquid phase and the resultant oxygen consumption rate (OCR). (B) Ratio of total choline/reference (total choline/ref) and lactate/reference (lactate/ref). (C) Glucose consumption rate (GCR) and lactate production rate (LPR) depicted in units of μmol/h for the entire culture. In each panel, the boundaries of the 4- and 24-h hypoxic episodes as well as the time of oxygen level step-up change are depicted. Dotted lines mark the beginning and end of the hypoxic episodes as well as the step-up in oxygen concentration.

hypoxic value within 36 h after reoxygenation. Panel C displays the profiles of glucose consumption rate (GCR) and lactate production rate (LPR) measured from medium samples that were removed from the perfusion fluid. Both rates increase during hypoxic episodes, and recover to their prehypoxic value within 36 h after reoxygenation.

The step-up in oxygen level is also depicted in Fig. 3 (Day 17 onward). Changes in the metabolic activity are attributed to both physiologic/metabolic changes as well as to an increase in viable cell numbers supported by a higher input DO level. The immediate and sharp increase in OCR is attributed to the increased oxygen consumption of existing viable cells; however, the subsequent gradual increase is due to an increase in the number of viable cells supported by the higher DO concentration. The NMR data show that with the increase in DO level, the ratio of total choline to reference increases continuously with time, while the lactate to reference ratio decreases for the first 2 days, followed by an increase as one approaches a new DO steady state. A similar profile is also observed for both the GCR and the LPR.

Given the large bioreactor volume and the observation that the metabolic activity of the culture increased dramatically during the first 6–7 days of culture, it is important to check for a stable metabolite signal distribution along the length of the bioreactor with the age of the culture. Figure 4 illustrates the distribution of the total choline/lactate ratio as a function of distance along the cylindrical axis coincident with the direction of flow at various times during the 32-day-long culture. The ratio of the total choline to lactate is used in order to correct for the basic B_1 field distribution of the RF coil. Since lactate intensity was determined to be symmetric about the center of the coil, at each time point, the above ratio reflects the distribution of total choline. The curves are normalized to a lactate concentration in the external media of 17.7 mM. Lactate concentration was measured analytically from samples of the medium collected periodically from the perfusion system, and was maintained constant by medium replenishment. The data in Fig. 4 show that during P1 and early P2 (Days 1 and 3) the ratio of total choline/lactate is nearly constant from input to output (slope of -0.002, -0.011 ratio units/cm), during late P2 (Day 5) a gradient is beginning to develop (-0.044 ratio units/cm), and finally during P3 (Day 16 and 30) the gradient is significant (-0.083 to -0.133 ratio units/cm). The increase in the ratio from Day 1 to 30 shows an increase in total choline relative to lactate. Indicated in Fig. 4 are also the input and output DO concentrations at each time of measurement (days).

DISCUSSION

Two questions that are critical for an implanted construct to sustain optimum function are: (1) is there a significant cell growth within the construct during the lifetime of the implant, and (2) do the cells experience conditions of nutrient deficiency as a result of either fibrotic overgrowth development or the

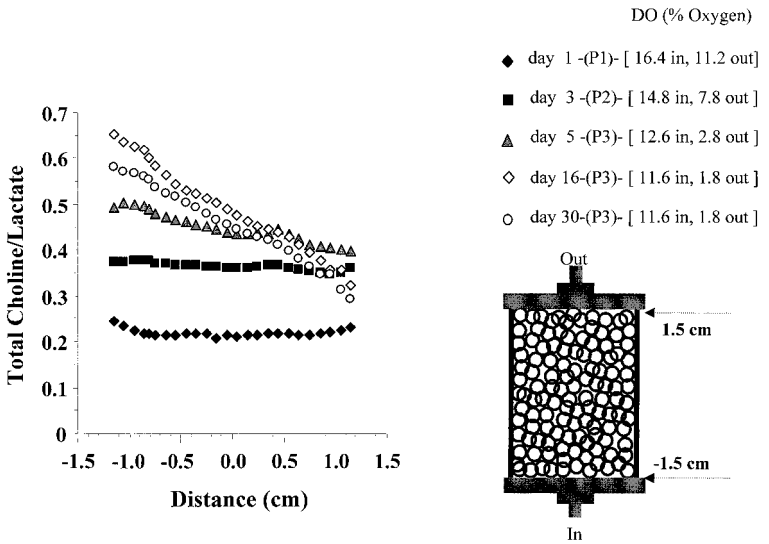

FIG. 4. 1D chemical shift imaging data of the total choline/lactate ratio (normalized to 17.7 mM lactate) versus distance along the bioreactor axis (the field of view for these experiments was 6 cm) acquired at different times during Culture I indicated in the figure. The corresponding input and output dissolved oxygen levels as percentage oxygen are shown in brackets with the associated culture phase designation P1, P2, or P3.

implantation procedure? It is apparent that either excessive growth or nutrient deficiency can be detrimental to the function of the implant. The ability to monitor *in vivo*, noninvasively, the function of a bioartificial pancreas might allow us to predict its potential to secrete insulin while the recipient patient is still normoglycemic. One technique that may fulfill this requirement is localized NMR spectroscopy. Given the fact that ^{1}H is the most sensitive NMR nucleus and that the capability to acquire ^{1}H NMR spectra is widely available in current MRI equipment, we set forth to investigate the utility of this nucleus for monitoring model tissue-engineered pancreatic constructs.

In addressing the first critical question raised above, it is apparent that the ratio of total choline to reference tracks the total number of viable metabolically active cells with their associated physiology. Assuming that OCR represents a measure of viable cells, then our observation in Fig. 2 that the major temporal changes in the total choline resonance correlate positively with changes in OCR infers that the total choline resonance can track the net cell growth of the system. This is supported by the observation that during P3 the ratio of total choline to reference is relatively stable. Although the cells continue to multiply, the net number of viable cells is the same. This has been previously demonstrated by hematoxylin/eosin-stained histology cross sections (*12*). The continuous division of cells, but lack of net cell growth, is attributed to the fact that a specific DO concentration supports only a fixed number of viable cells. As is shown in Fig. 3, following the step increase in $DO_{(in)}$ from ~9.0% oxygen (~64 mm Hg) to 23% oxygen (~163 mm Hg), the metabolic activity of the cells as reflected in the OCR reaches a new higher plateau. Total choline to reference also increases. This is primarily attributed to a net cell growth within the bioreactor. However, the presence of metabolic or physiological processes brought about by limiting concentrations of nutrients imposed by either specific environmental conditions or diffusional barriers that can either enhance or diminish this correlation cannot be discounted. These effects are expected to be particularly significant as heterogeneity in the cell population within the APA beads develops due to the continuous growth/death of the encapsulated cells (*12*, *16*, *24*). It should also be noted that the positive correlation between OCR and an NMR detectable intracellular metabolite is not unique to the total choline resonance, as similar results have been reported for ATP in APA-encapsulated βTC3 cells (*12*). However, the improved temporal resolution and signal-to-noise of the spectra, afforded by the increased sensitivity of the ^{1}H nucleus, make ^{1}H a more suitable nucleus for future *in vivo* experiments.

In addressing the second critical question, our data show that the total choline resonance is sensitive to changes in oxygen concentration. During all hypoxic episodes, the ratio of total choline to reference tracked the changes in %OCR, but with slower kinetics. Figure 3 clearly shows slower decline and recovery than %OCR. As the time of hypoxic insult increases, the time of recovery to the prehypoxic value increases. The time scale of choline recovery is on the order of 1.1 and 1.5 days for the 4-h and 24-h episodes, respectively. The fact that %OCR recovers immediately following reoxygenation to its prehypoxic values implies that the hypoxic episodes did not have a detrimental effect on the net viability of the culture. Therefore, the observed changes in total choline resonance during the hypoxic episodes are attributed to physiologic or metabolic causes and not to a change in net viability. This is a significant finding with implications that are wide ranging in areas of choline metabolism.

The first step in identifying a possible biochemical mechanism responsible for the change in total choline signal is to identify the component of the total choline resonance responsible for these changes. As we have stated under Results, extract spectra of βTC3 cells have identified PCho as the major component with 63.6 ± 4.0%, followed by GPC with 33.4 ± 4.0% and Cho with 3.0 ± 0.4%. Based on previous studies with ^{31}P NMR spectroscopy, the concentration of GPC does not change significantly with time during either 4-h or 24-h hypoxic episodes, whereas PCho does not change for the 4-h and declines during the 24-h episodes performed while the culture was in the middle of the P3 period (*17*). Since choline represents less than 5% of the total choline signal intensity, it is unlikely that it can contribute significantly to the observed decline. Therefore, the most probable scenario for the decrease in total choline during hypoxic episodes is a reduction of PCho. Owing to its sensitivity, proton NMR is able to detect small changes observed during 4-h episodes (~8%), whereas they are not detectable by ^{31}P NMR. During the 24-h episode, PCho intensity as determined by ^{31}P drops by 40% (*17*), in rough agreement with the proton data.

The enzymology underlying the changes of PCho metabolism is complex. Intracellular PCho concentration may be altered by a number of different mechanisms which include uptake of choline from the perfusion media and subsequent phosphorylation by choline kinase; activation of phospholipase C-induced release from phosphatidylcholine (PC); and GPC degradation by glycerophosphocholine hydrolase (*25*). The synthesis of PCho from exogenous choline has been demonstrated for several cell lines (*26, 27*). Although the direct demonstration of this process for βTC3 cells has not been studied in detail, there is evidence to suggest that PCho generation by phospholipase C activation might be present in βTC3 cells (*28*) as well as cholinergically stimulated pancreata (*29, 30*). Under hypoxic conditions, it has been suggested that the action of phospholipases leads to net phospholipid degradation with increases in choline, PCho, and possibly GPC concentrations (*31, 32*). Although an increase in PCho was hypothesized, a reduction of PCho was observed under conditions of hypoxia in ventricular myocytes (*31*). If we consider that the decline of PCho is due to a reduction in its overall rate of synthesis, then this reduction could be derived from one or a combination of the following: reduced rate of choline uptake from the media; a reduced choline kinase activity; or a reduced rate of choline phosphorylation due to a decrease in ATP concentration (ATP is required in the choline kinase step). In our ^{31}P studies, we have shown that both the PCho and the ATP intensity decrease during hypoxia (*16, 17*). It has also been shown that during hypoxia, leakage of PCho from the cytosol to the perfusion medium can occur (*33*).

A point of concern about our bioreactor system is the significant gradient in total choline signal observed during the period of metabolic plateau. We suggest that this gradient reflects one or a combination of the following: viable cell number, cell type fraction (proliferative, quiescent, and necrotic), and cell physiology at each point, from input to output of the bioreactor. It is known that proliferative cells have a higher steady-state level of PCho than quiescent or nonproliferative cells (*23*). Even though the 1D CSI experiment cannot separate the above contributions, it is plausible that the higher DO at the input of the bioreactor supports a larger number of viable more proliferative and more metabolically active cells than the DO at the output. Viewing the total choline/lactate ratio at specific positions along the bioreactor, it is found that this ratio takes on a quite different evolution with culture time. At the input, the ratio of total choline/lactate increases continuously with time, while at the output, it increases at first, followed by a decrease over time. At positions near the center, a limiting value is reached. When combined to give the overall global ratio, a near steady state is achieved. The temporal changes at the input and output locations are supportive of a larger number of metabolically healthy cells at the input versus the output.

In summary, our data demonstrate the utility of adiabatic solvent-suppression pulses for acquiring ^{1}H NMR spectra with a stability not possible by other methods for large bioreactors examined over prolonged periods of time. It establishes the dependence of the total choline signal, which is primarily phosphorylcholine, on the available oxygen concentration for the first time. For the field of tissue engineering, our results provide a foundation for the development of a noninvasive monitoring method to observe the function of cell-based tissue-engineered constructs *in vivo.*

MATERIALS AND METHODS

Cell Cultures and APA Encapsulation

βTC3 cells were obtained from the laboratory of Dr. Shimon Efrat (Department of Molecular Pharmacology, Albert Einstein College of Medicine, New York, NY). The cells were propagated as monolayers in T-flasks and cultured in Dulbecco's modified Eagle's medium (DMEM) (D-5648, Sigma Chemical Co., St. Louis, MO) supplemented with L-glutamine to a final concentration of 6 mM, 15% heat-inactivated horse serum, 2.5% fetal bovine serum, and 1% of penicillin/streptomycin solution as described previously (*11*). Only cells between passage number 32 to 47 were utilized for these experiments.

Encapsulation of βTC3 cells in APA beads was based on the initial protocol of Lim and Sun (*5*) that was modified to meet our present experimental requirements (*11*). Trypsinized cells were suspended in a 2% alginate solution (Kelco LV, San Diego, CA) and via an extrusion apparatus, droplets were allowed to fall in a 1.1% $CaCl_2$ solution producing calcium alginate beads. The beads were subsequently treated with poly-L-lysine (MW ~29,000, Sigma Chemical Co., St Louis, MO) and coated with alginate to form APA beads. Beads were 1.0 ± 0.2 mm (mean ± SD) in diameter and contained initially 7 ×

10^7 cells/mL alginate. Approximately 25 mL of APA beads was prepared and placed in spinner flasks for maintenance before loading into the bioreactor. All NMR experiments were initiated within 48 h after completion of the encapsulation protocol. The viability of the encapsulated cells, 24 and 48 h after completion of this procedure, has been reported by our group to range between 60 and 85%. No statistical differences in viability measured at these times are observed (*9, 34*).

Overall, two entrapped cultures were prepared for these studies, one that was maintained for 32 days (Culture I) and another that was maintained for 23 days (Culture II). A total of two 24-h and three 4-h hypoxic episodes were carried out for ^{1}H NMR studies.

Perfusion System

Beads with entrapped cells were placed in a 22-mL packed-bed bioreactor, resulting in a total number of 1.5×10^9 cells at the beginning of each experiment. The perfusion system, for which a detailed schematic is shown in a previous publication (*11*), consisted of three medium circulation loops. Only two circulation loops were used in this study: (1) a perfusion loop, in which medium was circulated through the bioreactor at a rate of 30 mL/min; and (2) a medium replenishment loop, which was used to constantly replace spent medium with fresh medium. Temperature sensors (Resistance Temperature Devices, Omega Engineering, Inc., Stamford, CT) and polarographic dissolved oxygen probes (Ingold, Wilmington, MA) were placed in flowthrough cells and positioned upstream and downstream of the bioreactor. Directly measured values of percentage air saturation were converted to percentage oxygen (100% air saturation is equal to 20% oxygen for 95% air/5% CO_2). All sensors were interfaced to a personal computer via an analog-to-digital board for repetitive data acquisition. In addition, the amount of medium removed was measured by weight online using an electronic balance interfaced to the data system, thus providing an accurate measure of the rate of replenishment. The perfusion system was operated at 37 ± 1°C initially in a batch mode (without replenishment) until the glucose concentration dropped to a desired level (10–16 mM). Medium replenishment was then initiated at a rate which maintained the residual glucose concentration in the perfusion loop at a predetermined level (Culture I, ~10 mM; Culture II, ~15 mM). The concentration of oxygen supplied to the headspace of the medium reservoir was maintained constant during the experiment by pumping incubator air. The supply of oxygen to the headspace combined with the oxygen demand of the cell culture and the leaks through the lines and other system components determined the bioreactor input oxygen level. Hypoxic episodes were carried out by pumping humidified 5% CO_2/95% N_2, while step-up in oxygen concentration was attained by pumping humidified 95% O_2/5% CO_2 into the headspace of the medium reservoir. Exposures to either reduced or increased dissolved oxygen concentrations were carried out during the period of metabolic and secretory steady state (P3).

Analytical Techniques

Lactate and glucose concentrations were determined with an Ektachem DT60 II analyzer (Eastman Kodak, Rochester, NY). The rates of glucose consumption (GCR) and lactate production (LPR) were determined by measuring the residual glucose and lactate concentrations in the perfusion loop and taking into account the concentrations of these species in the fresh medium and the rate of medium replenishment. The rate of oxygen consumption (OCR) was determined by measuring the difference between the input and output dissolved oxygen electrodes and multiplying this with the perfusion flow rate through the bioreactor. The Pharmed tubing used to connect the bioreactor between the input and output oxygen electrodes has negligible permeability to oxygen for the length used. However, oxygen consumption by the cells and line permeability to gases for all other lines leading to and from the medium resevoir as well as connectors preclude attaining a 0 or 95% oxygen level in our system.

Extracts of Monolayers and Beads for NMR Studies

Extraction of the intracellular milieu of βTC3 cells for assignment purposes was performed by the dual extraction method proposed by Tyagi *et al.* (*35*). Culture flasks were removed from the incubator and growth media aspirated. The cells were washed twice with ice-cold saline. Five milliliters of ice-cold methanol was added to each monolayer flask and allowed to stand for 5–10 min. The cells and cell debris were then scraped into 50-mL centrifuge tubes. Five milliliters of chloroform was added, followed by 5 mL of deionized water. The aqueous layer containing water-soluble intracellular metabolites was lyophilized after treatment with Chelex-100 (Bio-Rad Laboratories, Hercules, CA) and dissolved in a mixture of D_2O/H_2O (~300 μL) (5%/95%, v/v) in a 5-mm NMR tube. For the preparation of the NMR samples, 1–3 T-175 flasks were used. The extraction protocol for APA beads is similar to that described for monolayers, except that one additional saline wash was applied and the beads were allowed to equilibrate for an additional 10 min to allow media in the beads to diffuse out.

NMR Methods

Water-suppressed ^{1}H NMR spectra of perfused APA beads (total volume 22 mL) were obtained on a 4.7-T Sisco Varian 200/33 horizontal-bore spectrometer using a 12-cm-i.d. gradient insert. A copper foil loop–gap resonator 3 cm in diameter and 2.95 cm in height about the bioreactor and perpendicular to the main magnetic field acted as the transmit/receive coil. A 90°–TE/2–180°–acquisition spin-echo sequence was used, which employs BIR-4 adiabatic pulses ($\Delta\omega_{max}$ = 42 kHz) modified for solvent suppression, as first suggested by Garwood and co-workers (*36, 37*). Suppression was accomplished by introducing a free precession period within the pulses (solvent-suppressed adiabatic pulse, SSAP) in such a way as to

create minimum excitation at the water resonance frequency, and maximum excitation between the choline and lactate resonance. The length of the excitation pulse was 2.859 ms, and that of the refocusing pulse was 3.318 ms (the duration of free precession during the refocusing pulse was twice that during the excitation pulse). The repetition time was 2.39 s. The TE/2 echo time was chosen to be 128 ms. The excitation bandwidth maximum was centered at 2.00 ppm (540 Hz or 2.70 ppm upfield of the water resonance at 4.70 ppm). Use of this sequence resulted in the generation of an echo that contained optimum signal for the metabolites of interest and minimum signal for water. The digitized full-echo signal was obtained with a sweep width of 4000 Hz (2048 data points), zero filled to 4096 points, filtered with a Gaussian filter constant, gf, of 0.038 s defined in $\exp(-(t/\mathrm{gf})^2)$, Fourier transformed, and fit in the frequency domain by Lorentzian model functions for each resonance in the frequency domain by routines supplied with the Sisco/Varian software. Each *in vitro* spectrum was the result of 64 acquisitions. 1D CSI was carried out at various times over the history of the culture. For 1D CSI, 32 phase encoding steps were applied and the data were zero filled to 128 in the phase encoding direction. With a field of view of 6 cm, this results in a resolution of 0.94 mm along the flow axis.

ACKNOWLEDGMENTS

The authors gratefully acknowledge support in part from the NIH (DK47858), the NSF (BES9410703), and the ERC Program of the National Science Foundation under Award EEC9731643. We also acknowledge the excellent skilled technical assistance of Mrs. Inge Rask.

REFERENCES

1. S. Darquy and G. Reach, Immunoisolation of pancreatic β cells by microencapsulation: An *in vitro* study, *Diabetologia* **28,** 776–780 (1985).
2. P. Soon-Shiong, Z. N. Lu, I. Grewal, R. P. Lanza, and W. Clark, An *in vitro* method of assessing the immunoprotective properties of microcapsule membranes using pancreatic and tumor cell targets, *Transplant. Proc.* **22,** 754–755 (1990).
3. M-Y. Fan, Z-P. Lum, X-W. Fu, L. Levesque, I. T. Tai, and A. M. Sun, Reversal of diabetes in BB rats by transplantation of encapsulated pancreatic islets, *Diabetes* **39,** 519–522 (1990).
4. P. E. Lacy, O. D. Hegre, A. Gerasimidi-Vazeou, F. T. Gentile, and K. E. Dionne, Maintenance of normoglycemia in diabetic mice by subcutaneous xenografts of encapsulated islets, *Science* **254,** 1782–1784 (1991).
5. F. Lim and A. M. Sun, Microencapsulated islets as bioartificial endocrine pancreas, *Science* **210,** 908–910 (1980).
6. P. Soon-Shiong, E. Feldman, R. Nelson, J. Komtebedde, O. Smidsrod, G. Skjak-Braek, T. Espevik, R. Heintz, and M. Lee, Successful reversal of spontaneous diabetes in dogs by intraperitoneal microencapsulated islets, *Transplantation* **54,** 769–774 (1992).
7. S. J. Sullivan, T. Maki, K. M. Borland, M. D. Mahoney, B. A. Solomon, T. E. Muller, A. P. Monaco, and W. Chick, Biohybrid artificial pancreas: Long-term implantation studies in diabetic, pancreatectomized dogs, *Science* **252,** 718–721 (1991).
8. P. Soon-Shiong, R. E. Heintz, N. Merideth, Q. X. Yao, Z. Yao, T. Zheng, M. Murphy, M. K. Moloney, M. Schmehl, M. Harris, R. Mendez, R. Mendez, and P. A. Sandford, Insulin independence in a type I diabetic patient after encapsulated islet transplantation, *Lancet* **343,** 950–951 (1994).
9. A. Sambanis, K. K. Papas, P. C. Flanders, R. C. Long, Jr., H. Kang, and I. Constantinidis, Towards the development of a bioartificial pancreas: Immunoisolation and NMR monitoring of mouse insulinomas, *Cytotechnology* **15,** 351–363 (1994).
10. I. Constantinidis and A. Sambanis, Towards the development of artificial endocrine tissues: ^{31}P NMR spectroscopic studies of immunoisolated, insulin-secreting AtT-20 cells, *Biotechnol. Bioeng.* **47,** 431–443 (1995).
11. K. K. Papas, R. C. Long, Jr., I. Constantinidis, and A. Sambanis, Role of ATP and P_i in the mechanism of insulin secretion in the mouse insulinoma βTC3 cell line, *Biochem. J.* **326,** 807–814 (1997).
12. K. K. Papas, R. C. Long, Jr., I. Constantinidis, and A. Sambanis, Towards the development of a bioartificial pancreas. I. Long-term propagation and basal and induced secretion from entrapped βTC3 cell cultures, *Biotechnol. Bioeng.* **66,** 219–230 (1999).
13. I. Constantinidis, N. E. Mukundan, M. Gamcsik, and A. Sambanis, Towards the development of a bioartificial pancreas: A ^{13}C NMR study on the effects of alginate/poly-L-lysine/alginate entrapment on glucose metabolism by βTC3 mouse insulinoma cells, *Cell. Mol. Biol.* **43,** 721–729 (1997).
14. N. E. Mukundan, P. C. Flanders, I. Constantinidis, K. K. Papas, and A. Sambanis, Oxygen consumption rates of free and alginate-entrapped βTC3 mouse insulinoma cells, *Biochem. Biophys. Res. Commun.* **210,** 113–118 (1995).
15. K. K. Papas, R. C. Long, Jr., I. Constantinidis, and A. Sambanis, Effects of oxygen on the metabolic and secretory activities of βTC3 cells, *Biochim. Biophys. Acta* **1291,** 163–166 (1996).
16. K. K. Papas, R. C. Long, Jr., I. Constantinidis, and A. Sambanis, Towards the development of a bioartificial pancreas. II. Effects of oxygen on long-term entrapped βTC3 cell cultures, *Biotechnol. Bioeng.* **66,** 231–237 (1999).
17. K. K. Papas, R. C. Long, Jr., I. Constantinidis, and A. Sambanis, Effects of short-term hypoxia on the bioenergetics and insulin secretion of alginate entrapped mouse insulinoma βTC3 cells, *Cell Transplant.,* in press (2000).
18. R. Callies, M. E. Jackson, and K. M. Brindle, Measurements of the growth and distribution of mammalian cells in a hollow-fiber bioreactor using nuclear magnetic resonance imaging, *Bio/Technology* **12,** 75–78 (1994).
19. U. Pilatus, H. Shim, D. Artemov, D. Davis, P. C. D. van Zijl, and J. D. Glickson, Intracellular volume and apparent diffusion constants of perfused cancer cell cultures, as measured by NMR, *Magn. Reson. Med.* **37,** 825–832 (1997).
20. P. Weybright, K. Millis, N. Campbell, D. G. Cory, and S. Singer, Gradient, high-resolution, magic angle spinning ^{1}H nuclear magnetic resonance spectroscopy of intact cells, *Magn. Reson. Med.* **39,** 337–345 (1998).
21. M. Gueron, P. Plateau, and M. Decorps, Solvent signal suppression in NMR, *Prog. NMR Spectrosc.* **23,** 135–209 (1991).
22. J. K. Nicholson, P. J. D. Foxall, M. Spraul, R. D. Farrant, and J. C. Lindon, 750 MHz ^{1}H and ^{13}C NMR spectroscopy of human blood plasma, *Anal. Chem.* **67,** 793–811 (1995).
23. S. M. Ronen, E. Rushin, and H. Degani, Lipid metabolism in large T47D human breast cancer spheroids: ^{31}P and ^{13}C NMR studies of choline and ethanolamine uptake, *Biochim. Biophys. Acta* **1138,** 203–212 (1992).

24. I. Constantinidis, I. Rask, R. C. Long, Jr., and A. Sambanis, Effects of alginate composition on the metabolic, secretory, and growth characteristics of entrapped βTC3 mouse insulinoma cells, *Biomaterials* **20,** 2019–2027 (1999).

25. K. K. Bhakoo, S. R. Williams, C. L. Florian, H. Land, and M. D. Noble, Immortalization and transformation are associated with specific alterations in choline metabolism, *Cancer Res.* **56,** 4630–4635 (1996).

26. P. F. Daly, R. C. Lyon, P. J. Faustino, and J. S. Cohen, Phospholipid metabolism in cancer cells monitored by ^{31}P NMR spectroscopy, *J. Biol. Chem.* **262,** 14875–14878 (1987).

27. R. J. Gillies, J. A. Barry, and B. D. Ross, In vitro and in vivo ^{13}C and ^{31}P NMR analysis of phosphocholine metabolism in rat glioma cells, *Magn. Reson. Med.* **32,** 310–318 (1994).

28. G. Baffy, L. Yang, B. A. Wolf, and J. R. Williamson, G-protein specificity in signaling pathways that mobilize calcium in insulin secreting βTC3 cells, *Diabetes* **42,** 1878–1882 (1993).

29. M. W. Banschbach, R. L. Geison, and M. Hokin-Neaverson, Effects of cholingeric stimulation on levels and fatty acid composition of diacylglycerols in mouse pancreas, *Biochim. Biophys. Acta* **663,** 34–45 (1981).

30. J. H. Exton, Signaling through phosphatidylcholine breakdown, *J. Biol. Chem.* **265,** 1–4 (1990).

31. T. Myremel, T. K. Steigen, E. Bjordal, and T. S. Larsen, Phosphatidylcholine metabolism in hypoxic and phospholipase C exposed rat ventricular myocytes, *Can. J. Physiol. Pharmacol.* **71,** 840–847 (1993).

32. Z. M. Bhujwalla, D. C. Shungu, and J. D. Glickson, Effects of blood flow modifiers on tumor metabolism observed in vivo by proton magnetic resonance spectroscopic imaging, *Magn. Reson. Med.* **36,** 204–211 (1996).

33. W. J. Van Blitterswijk, H. Hilkmann, J. deWidt, and R. L. van der Bend, Phospholipid metabolism in bradykinin-stimulated human fibroblasts. II. Phosphatidylcholine breakdown by phospholipase C and D; involvement of protein kinase C, *J. Biol. Chem.* **266,** 10344–10350 (1991).

34. J. P. Benson, K. K. Papas, I. Constantinidis, and A. Sambanis, Towards the development of a bioartificial pancreas. Effects of poly-L-lysine on alginate beads with βTC3 cells, *Cell Transplant.* **6,** 395–402 (1997).

35. R. K. Tyagi, A. Azrad, H. Degani, and Y. Salomon, Simultaneous extraction of cellular lipids and water-soluble metabolites: Evaluation by NMR spectroscopy, *Magn. Reson. Med.* **35,** 194–200 (1996).

36. M. Garwood and Y. Ke, Symmetric pulses to induce arbitrary flip angles with compensation for RF inhomogeneity and resonance offsets, *J. Magn. Reson.* **94,** 511–525 (1991).

37. B. D. Ross, H. Merkle, K. Hendrich, R. S. Staewen, and M. Garwood, Spatially localized *in vivo* ^{1}H magnetic resonance spectroscopy of an intracerebral rat glioma, *Magn. Reson. Med.* **23,** 96–108 (1992).